Six-Wavelength-Switchable SLM Thulium-Doped Fiber Laser Enabled by Sampled FBGs and 3 × 3 Coupler Based Dual-Ring Compound Cavity Filter

Dan Cheng, Fengping Yan, Ting Feng, Luna Zhang, Wenguo Han, Qi Qin, Ting Li, Zhuoya Bai, Dandan Yang, Ying Guo, Wei Wang, and Yan Bai

***Abstract*—A switchable and tunable six-wavelength single-longitudinal mode (SLM) thulium-doped fiber laser in the 2050 nm band is proposed and experimentally demonstrated. Two cascaded sampled fiber Bragg gratings (SFBGs), acted as an integrated six-channel reflector, are to define the lasing wavelength channels in a multi-wavelength switchable fiber laser for the first time. The switchability of the fiber laser was realized by polarization-dependent loss modulation. SLM lasing in each channel was guaranteed by a novel passive dual-ring compound cavity (DRCC), composed of two symmetric 3 × 3 optical couplers (OCs). Six single-wavelength operations are easily obtained and switched, with the high optical signal-to-noise ratios of >71 dB, >72 dB, >62 dB for λ_{11}–λ_{13} and > 65 dB, >61 dB, >59 dB for λ_{21}–λ_{23}, respectively. The maximum power and wavelength fluctuations are as low as 0.56 dB and 0.01 nm, respectively. The measured laser linewidths ranged from 7.5 to 9.2 kHz, calculated by the β-separation line method based on the measured frequency noise spectra. Nine switchable dual-wavelength operations with different wavelength intervals and two triple-wavelength operations were also obtained. Our proposed fiber laser has great potential in free-space optical communication.**

***Index Terms*—Thulium-doped fiber laser, single-longitudinal-mode, laser linewidth, sampled fiber Bragg grating.**

Manuscript received December 1, 2021; revised January 9, 2022; accepted January 25, 2022. Date of publication February 1, 2022; date of current version February 28, 2022. This work was supported in part by the National Natural Science Foundation of China under Grants 61827818, 61620106014, 61975049, 62005013, and 61975105, in part by the Hebei Provincial Natural Science Foundation for Outstanding Young Scholars under Grant F2020201001, and in part by the Science and Technology Research Project of Higher Education in Hebei Province under Grant QN2021050. *(Corresponding authors: Fengping Yan; Ting Feng.)*

Dan Cheng, Fengping Yan, Wenguo Han, Qi Qin, Ting Li, Zhuoya Bai, Dandan Yang, Ying Guo, and Wei Wang are with the School of Electronic and Information Engineering, Beijing Jiaotong University, Beijing 100044, China (e-mail: dancheng621@hotmail.com; fpyan@bjtu.edu.cn; 14111021@bjtu.edu.cn; 19111034@bjtu.edu.cn; 19111024@bjtu.edu.cn; 16111003@bjtu.edu.cn; 2554332431@qq.com; 18111014@bjtu.edu.cn; 15111006@bjtu.edu.cn).

Ting Feng is with the Photonics Information Innovation Center, Hebei Provincial Center for Optical Sensing Innovations, College of Physics Science and Technology, Hebei University, Baoding 071002, China (e-mail: wlxyft@hbu.edu.cn).

Luna Zhang is with the Key Lab of Solid State Laser, Technical Institute of Physics and Chemistry, Chinese Academy of Sciences, Beijing 100190, China (e-mail: zhangluna@mail.ipc.ac.cn).

Yan Bai is with the College of Electrical Engineering, Hebei University of Architecture, Zhangjiakou, Hebei 075000, China (e-mail: by2130@hebiace.edu.cn).

Digital Object Identifier 10.1109/JPHOT.2022.3147223

I. Introduction

SINGLE–longitudinal-mode (SLM) thulium-doped fiber lasers (TDFLs) have gained intense research interest due to their promising scientific, technical, and military application potential. The broad emission range (1660–2200 nm) of TDFL radiation not only falls in the eye-safe spectral region but also overlaps with the absorption lines of various atmospheric gases. This allows for the fabrication of 2 μm SLM fiber lasers that can be widely applied in high-resolution sensing, especially for coherent Doppler lidar wind detection [1]–[3]; Moreover, this emission range covers the atmospheric transparency window, where the permissible power transmission for light in the free-space can be several orders of magnitude higher than other wavelength bands. In particular, the optical power transmittance of light at ∼2050 nm is over 80% [4], enabling the use of SLM fiber lasers in the 2050 nm band in free-space optical communications and the atmospheric Doppler lidar.

Thus far, most works involving the 2 μm band focus on the 1900–2000 nm region, which is the high gain band of thulium-doped fibers (TDFs) [5]–[8]. However, SLM TDFLs in the 2050 nm band are still rarely reported. Since the laser wavelength of 2050 nm is at the edge of the gain region of TDFs, this is challenging for SLM lasers in the 2050 nm band with short linear cavity configurations. Apart from replacing the gain fiber with Ho-doped fiber [9], [10], this problem could be solved by using the ring-cavity configuration with an extended length of Tm-doped fiber to provide sufficient gain in the 2050 nm band. Compared with the SLM laser with a short cavity, the ring cavity configuration is more flexible and tunable, since it allows tunable components or additional wavelength selectors to be installed in the cavity. Through this, switchable or tunable single- or multi-wavelength operation can be realized. Fiber laser at 2050 nm with multi-wavelength channels, each being in the SLM state, are highly expected to be used in next-generation LiDARs that require a seed laser with wavelength tunability, wavelength stability, and narrow linewidth as well as in wavelength division-multiplexing (WDM) free-space optical communication.

Benefiting from the rapid development of lasers in the C- and L-bands, the current technique used to realize wavelength-switchable SLM lasing can also be used as a reference for lasers in the 2 μm band. Typical laser configurations involve a multi-channel optical filter to select lasing wavelengths and a switching

mechanism to control the operation mode. The multi-channel optical filter can be one of the following: a photonic crystal fiber based Mach-Zehnder interferometer [11], a superimposed FBG [12], [13], a wideband chirped Moiré FBG filter [14], [15], a sample fibered Bragg grating (SFBG) or a polarization-maintaining (PM) SFBG [16], [17], a Sagnac interferometer [18], a few-mode fiber with core-offset structure [19], etc. The wavelength switching mechanism can be one of the following: tunable-filter scanning [20], polarization-dependent loss (PDL) [21], polarization controlling [17], or nonlinear polarization rotation (NPR) [16], [22], etc. To further enable SLM lasing for the wavelength-switchable laser, it is critical to find effective mode-selection mechanisms against the resulting small FSR due to the elongated laser cavity length. Effective mode-selection techniques include the use of ultra-narrow bandwidth filters or an unpumped doped fiber as a self-tracking narrowband reflection filter [23], [24], and the incorporation of the compound-cavity or the multi-ring compound cavity (MR-CC) [12], [13], [25]–[28]. The fiber rings used in MR-CC are generally based on optical couplers (OCs), which makes this method a more affordable and easier alternative for use in the 2 μm band, where there is a lack of optimized components.

Herein, we propose a switchable and tunable six-wavelength SLM TDFL in the 2050 nm band. In our laser configuration, the novel multi-channel optical filter is fabricated by two identical cascaded SFBGs, one of which is clamped on a micro-displacement platform. The wavelength switching mechanism is achieved by introducing PDL modulation, and a novel passive dual-ring compound cavity (DRCC) is proposed to enable SLM lasing. The maximum OSNR of the obtained lasing wavelengths is ~72.11 dB and the measured laser linewidths range from 7.5 to 9 kHz. Furthermore, the TDFL can produce nine dual-wavelength and two triple-wavelength lasing outputs. To the best of our knowledge, this is the first switchable multi-wavelength SLM Tm-doped fiber laser operated at ~2050 nm. The preferable output performance enables the TDFL promisingly to be used in next-generation lidar systems as well as in WDM free-space optical communication.

II. Experimental Setup and Principles

A. Laser Configuration

The experimental setup of the laser is depicted in Fig. 1. The Tm-doped double-clad fiber (TDF, Nufern SM-TDF-10P/130-M) was chosen to be 4.5 m long to provide enough gain and was pumped by a laser diode centered at 793 nm with up to 12 W power through a fiber combiner (FC). Two cascaded sampled fiber Bragg gratings (SFBGs) and drop-in polarization controllers (DI-PCs), serving as a multi-channel reflection filter (MCRF) and polarization-dependent components, were connected with a three-port optical circulator. A micro-displacement platform clamped the second SFBG to adjust the reflection wavelengths. The distance, which included DI-PC2 between SFBG1 and SFBG2, was about 30 cm. The circulator spliced in the active main ring cavity (AMRC) also ensured the unidirectional oscillation of the laser. A subsequent optical fiber polarizer (OFP), which allowed for a certain polarization state of light to pass through, was spliced at port 3 of the circulator. Wavelength switching between SFBG1 and SFBG2 was realized through the coordination of DI-PCs, SFBGs, and OFP. A passive dual-ring compound cavity (DR-CC), which was composed of two 3 × 3 symmetric optical couplers (OCs), was nested in the AMRC to enable the SLM operation of the laser. The cavity lengths of ring 1 and ring 2 of the DRCC were 2.43 and 2.45 m, respectively. Ultimately, a 1 × 2 OC extracted 10% of the resulting SLM lasing. The AMRC composed of SFBG1 (AMRC1) was 12.5 m, and the AMRC composed of SFBG2 (AMRC2) was about 12.8 m.

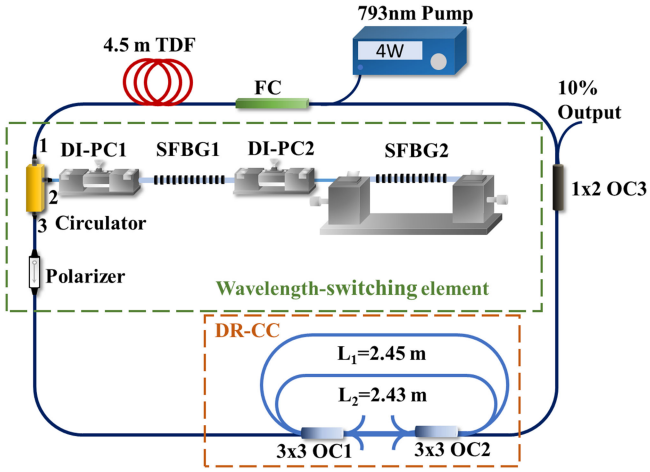

Fig. 1. Schematic diagram of the wavelength-switchable SLM laser with a passive DRCC. SFBG: sampled fiber bragg grating; TDF: Tm-doped fiber; DI-PC: drop-in polarization controller; DRCC: dual-ring compound cavity; OC: optical coupler.

Two SFBGs used as the MCRF were both fabricated in-house using the phase mask method with a uniform phase mask (period $\lambda = 1423.7$ nm) and a homemade sampling mask (grating length $L = 20$ mm, sampling period $d = 1$ mm, duty-cycle $t = 0.5$). They were both directly written by a 248 nm KrF excimer laser, and the grating lengths were both 20 mm [17]. The calculated central Bragg wavelength λ_B and wavelength separation $\Delta\lambda$ of both SFBGs are respectively ~2050.12 nm and ~1.46 nm, according to $\lambda_B = 2n_{eff}\Lambda$ and $\Delta\lambda = {\lambda_B}^2/(2n_{eff}d)$ for the determined phase mask period and the sampling period. The reflection and transmission spectra of SFBG1 and SFBG2 are shown in Fig. 2, which were measured using a homemade amplified spontaneous emission (ASE) light source and an OSA (YOKOGAWA AQ6375) with a resolution of 0.05 nm. For each SFBG, three reflecting channels were obtained. The wavelength, reflectivity, and reflecting bandwidth (RB) of each reflecting channel of SFBG1 and SFBG2 are listed in Table I. The wavelengths of two SFBGs were not completely consistent, which can be attributed to the stress differences created during fabrication. Note that, in our experiments, the SFBG2 was stretched for wavelength tuning. Actually, either of the SFBGs or both of them can be stretched, and we believe that the wavelength and wavelength-interval tunabilities can be further improved if both SFBGs are stretched.

Wavelength switching can be realized through the coordination of DI-PCs, SFBGs, and OFP. When the ASE light with an

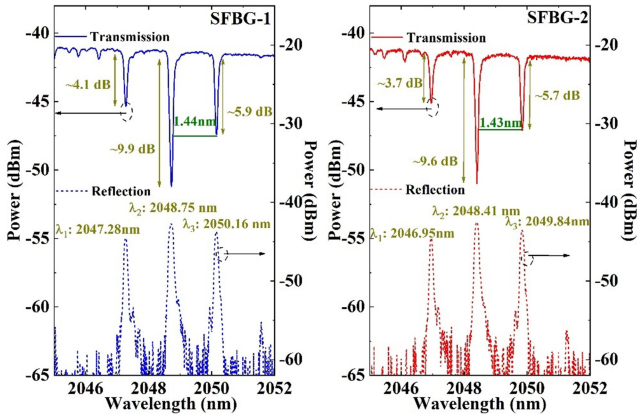

Fig. 2. Reflection and transmission spectra of SFBG1 and SFBG2.

TABLE I
THE WAVELENGTH, REFLECTIVITY, AND REFLECTING BANDWIDTH (RB) FOR DIFFERENT CHANNELS OF SFBG1 AND SFBG2

	SFBG-1		
	λ_{11}	λ_{12}	λ_{13}
Wavelength (nm)	2047.28	2048.75	2050.12
Reflectivity (%)	61.1	89.77	74.3
RB (nm)	0.12	0.16	0.13
	Tunable SFBG-2		
	λ_{21}	λ_{22}	λ_{23}
Wavelength (nm)	2046.96	2048.41	2049.84
Reflectivity (%)	57.34	89.04	73.08
RB (nm)	0.11	0.15	0.14

arbitrary polarization state generated from the gain fiber passes by the port 2 of the circulator, the state of polarization (SOP) of light will be changed by DI-PC1 and DI-PC2. Then the lights with their own corresponding wavelengths are reflected at the SFBGs, with their SOPs rotated again by the corresponding DI-PC in front of each SFBG, and injected into the subsequently connected OFP after the circulator. As the layout of OFP is fixed, lights with different SOPs at different wavelengths determined by SFBGs suffer different polarization-dependent losses (PDLs) after passing through the OFP. In our laser configuration, the PDLs (λ_{11}–λ_{13}) of SFBG1 are mainly determined by DI-PC1, and the PDLs (λ_{21}–λ_{23}) of SFBG2 are further decided by DI-PC2. Given the laser-oscillating condition, the laser can be built at a wavelength where the single-loop propagation loss is the lowest. Here, the total loss for each wavelength includes cavity loss and PDL [21], [29]. Switchable lasing among the six wavelengths determined by SFBGs can be obtained by adjusting the PDL through tuning the DI-PCs and based on the gain competition effect of the homogeneous broadening rare-earth-doped fiber. It is worth noting that the DI-PCs were adjusted in order, by which to obtain the individual control of the SOP of each light reflected by each SFBG. More specifically, the PDL of the light reflected by SFBG1 should be controlled first as it was only determined by DI-PC1. Then, further controlling the PDL of the SFBG2 by tuning the DI-PC2, in the meantime, the DI-PC1 was kept unchanged and the PDL of SFBG1 would not be influenced when controlling the PDL of SFBG2. Furthermore, the adjustment of the DI-PC was not quantitative. Therefore, the only way to determine whether the PDL was adjusted enough to switch to another lasing mode was to observe the output laser spectrum, rather than adjusting the 3-paddle PC to a certain angle for each lasing mode. Note that, due to the significant bending loss in the 2.05 μm band compared to other wavelength bands and the generally small diameters of the coiled fibers in the paddles of the 3-paddle PC, the bending loss brought in by the small coiled diameter of the fiber in the paddles was detrimental for lasing in the 2.05 μm band. We have confirmed that the use of 3-paddle PCs in our laser configuration could lead to no lasing, so two DI-PCs were used alternatively.

B. Principle of SLM Lasing

The DRCC is the core element for SLM selection for the proposed laser configuration. In the previous proposed passive subring cavities [30], [31], the fiber rings were generally made using 2×2 OCs. In this work, a DRCC made of two symmetric 3×3 OCs for the first time was used in a novel approach for the realization of SLM specificity in our laser. The corresponding longitudinal-mode spacings of AMRC1 and AMRC2 were about 16.7 and 16.3 MHz, respectively. It was also found that the maximum reflection bandwidth of the SFBGs at each reflection channel was 0.16 nm, corresponding to a frequency bandwidth of about 11.4 GHz at 2050 nm, which indicates that the DRCC should guarantee only one mode to be selected from the ~700 modes in each reflection bandwidth. To realize SLM selection from the dense longitudinal modes of AMRC by DRCC, the following two aspects need to be satisfied. First, the effective free-spectral range (FSR) of DRCC should be comparable with the reflection bandwidth of SFBG, which allows only one effective transmission channel of DRCC to be dropped in each reflection bandwidth of SFBG. As the difference in cavity length between ring 1 and ring 2 of the DRCC was 0.2 cm, according to the Vernier effect [32], when the difference in cavity length between the two DRCC rings is much less than their cavity lengths, the effective FSR of DRCC is given as

$$FSR = c/(n_{eff} \cdot \Delta L) \tag{1}$$

where $c = 3 \times 10^8$m/s is the speed of light, $n_{eff} = 1.44$ is the effective refractive index, and ΔL is the difference in the cavity length. The effective FSR of the DRCC was calculated as 10.42 GHz, which was slightly less than the reflection bandwidth of the SFBGs. Second, the passband Δv of the DRCC should be comparable with the FSR of the AMRC, which guarantees that only one longitudinal mode is located at the passband of the DRCC. The passband bandwidth of the DRCC can be calculated according to the following equation [13], [26]:

$$\Delta v = \frac{c\delta}{2\pi n_{eff} L_1} \tag{2}$$

where L_1 denotes the cavity length of the longest resonator of DRCC (ring 1), which determine the minimum passband bandwidth of the compound cavity. δ denotes the one-way loss

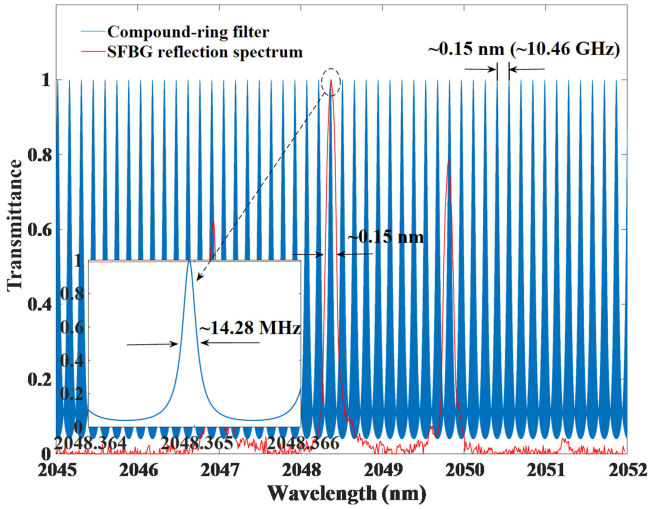

Fig. 3. Transmission spectrum of the DRCC filter, the inset is the zoomed-in transmission spectrum of DRCC filter at the central wavelength of SFBG.

of the DRCC, which is expressed by

$$\delta = \ln(\frac{I_i}{I_o}) \tag{3}$$

where I_o and I_i are the output and input light intensities, respectively. The symmetric 3 × 3 optical fiber coupler is described by the matrix of

$$T = \frac{1}{\sqrt{3}} \begin{pmatrix} 1 & \exp\frac{i2\pi}{3} & \exp\frac{i2\pi}{3} \\ \exp\frac{i2\pi}{3} & 1 & \exp\frac{i2\pi}{3} \\ \exp\frac{i2\pi}{3} & \exp\frac{i2\pi}{3} & 1 \end{pmatrix} \tag{4}$$

The one-way loss δ was calculated as ∼1.19 using the given transmission matrix and the 0.2 dB insertion loss of two OCs. The passband Δv was calculated as ∼16.11 MHz. Fig. 3 shows the simulated transmittance of the DRCC filter, using the same parameters with them in its fabrication in the experiment, based on the theoretical method described in Ref. [12]. For comparison, the reflection spectrum of the SFBG1 is also plotted in the figure. As can be seen, the effective FSR of the comb spectrum generated by the DRCC is ∼0.15 nm (∼10.46 GHz @ 2050 nm band), which is in agreement with the calculated effective FSR and is comparable to the FWHM bandwidth of each SFBG's reflection channel. The inset is a zoomed-in spectrum of the main passband from the DRCC comb spectrum. The FWHM bandwidth of the passband is ∼14.28 MHz, which is comparable to the estimated value ∼16.11 MHz and less than the longitudinal-mode spacing of the AMRC1 and AMRC2 (16.7 MHz and 16.3 MHz). Those can guarantee that only one longitudinal-mode can oscillate in each reflection channel of the SFBGs.

III. Experimental Results and Discussion

All measurements were carried out at room temperature with air conditioning constantly running, and no extra vibration isolation and temperature compensation techniques were employed for the proposed laser system, which was placed together with

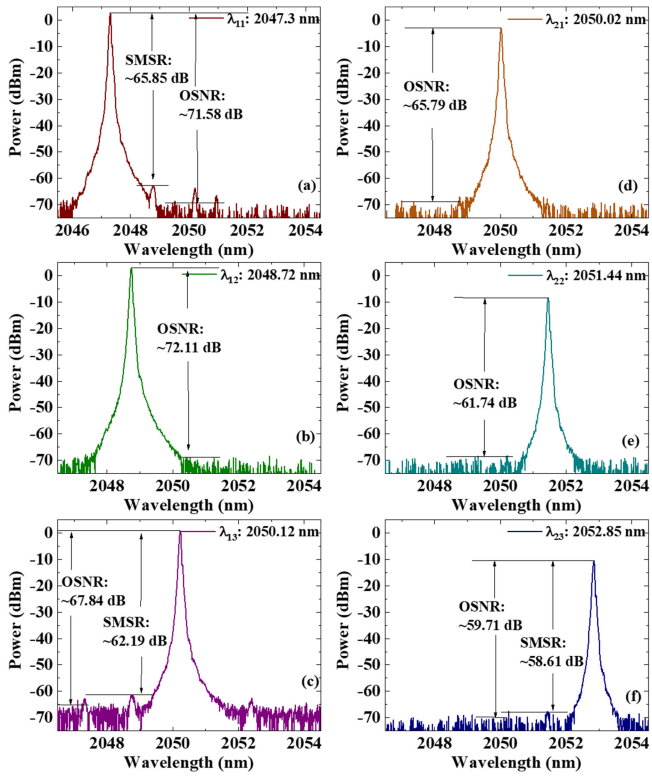

Fig. 4. Spectra of the obtained lasing outputs corresponding to each channel of SFBG1 and SFBG2 at wavelengths of (a) 2047.3 nm, (b) 2048.72 nm, (c) 2050.12 nm, (d) 2050.02 nm, (e) 2051.44 nm, and (f) 2052.85 nm. OSNR: optical signal-to-noise ratio. SMSR: side-mode suppression ratios.

the pump source on the ordinary table. The laser threshold was measured to be 3 W when the pump power was higher than that, and by adjusting DI-PCs carefully, stable single wavelength SLM operation switching between all reflection wavelengths of the SFBGs and multi-wavelength operation could be obtained. The outstanding performance of our proposed laser regardless of the operation modes was demonstrated as follows:

A. Switchable Single Wavelength Operation

The pump power was fixed at 3.8 W and the central wavelength of SFBG2 was tuned to 2051.44 nm. By adjusting the DI-PC1 and DI-PC2, six wavelengths were obtained respectively lasing at λ11 = 2047.3 nm, λ12 = 2048.7 nm, λ13 = 2050.12 nm, λ21 = 2050.02 nm, λ22 = 2051.44 nm and λ22 = 2052.85, which are corresponding to the six reflection channels of SFBG1 and SFBG2. The spectrum of each wavelength was measured by OSA with a resolution of 0.05 nm and a data sampling interval of 0.01 nm. For each lasing wavelength, the spectra of OSA scans repeated ten times with an interval of 2 min were measured. The typical spectrum of eleven measured output spectra (the first scanning was included) of each lasing wavelength is shown in Fig. 4. The 3-dB bandwidths of all the obtained lasing wavelengths were ∼0.078, which is near the OSA resolution. The optical signal-to-noise ratios (OSNRs) of the lasing from SFBG1 refection channels were respectively 71.58, 72.11, and 67.84 dB, while the OSNRs of the lasing

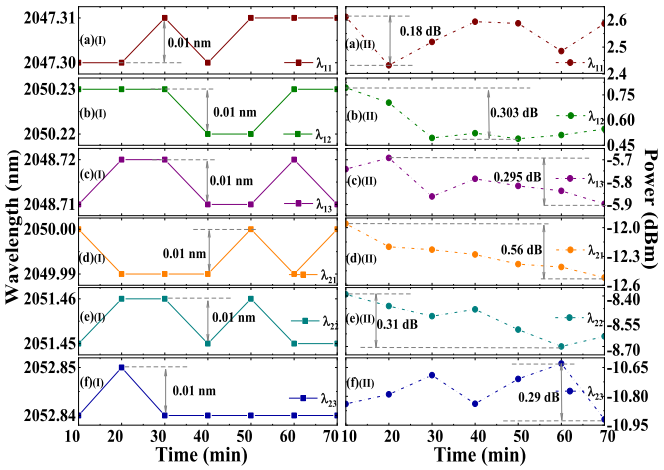

Fig. 5. Wavelength and power fluctuations over 60 min lasing at (a) (I, II) 2047.3 nm, (b) (I, II) 2048.72 nm, (c) (I, II) 2050.12 nm, (d) (I, II) 2050.02 nm, (e) (I, II) 2051.44 nm, and (f) (I, II) 2052.85 nm.

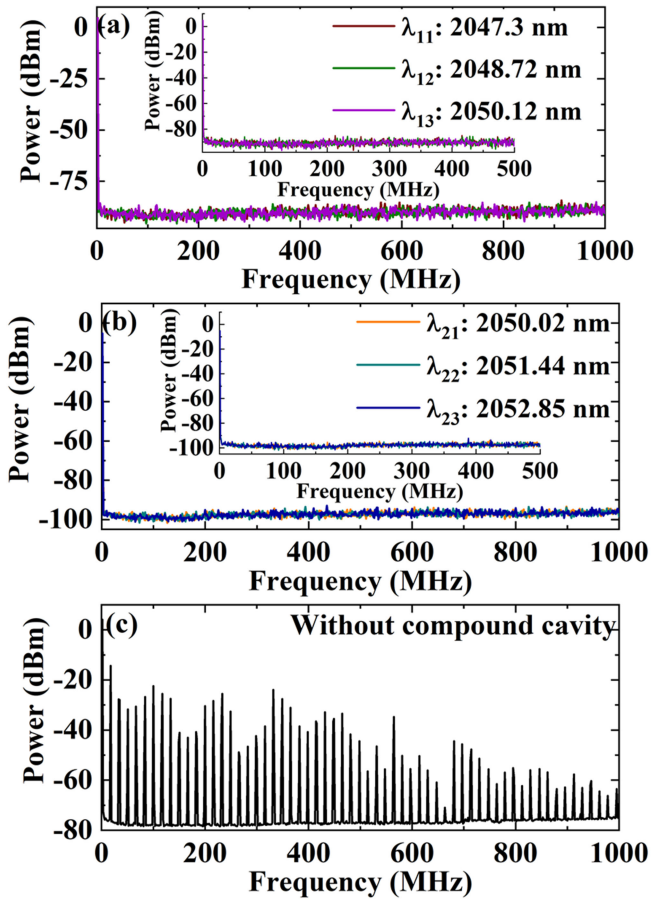

Fig. 6. Self-homodyne RF spectra measured by ESA for every lasing wavelength reflected by (a) SFBG1 and (b) SFBG2 of the proposed TDFL measured in the range of 0–500 MHz and 0–1GHz. (c) RF beating spectra of the laser without the DRCC filter.

from the SFBG2 refection channels were 65.79, 61.74, and 59.71 dB. As the gain provided by the TDF after 2010 nm declined continuously, the OSNRs of lasing at the SFBG2 channels were lower than them for SFBG1. Nevertheless, the overall high OSNRs indicated the high oscillating quality of our proposed laser and the decent mode selection capability of the DRCC. Following, the stability of the proposed TDFL was investigated further over a 60-min experimental period with an interval of 10 min (Fig. 5). Within the measurement results for the six lasing wavelengths, the minimum and maximum power fluctuations between them were 0.18 and 0.56 dB, respectively, and the wavelength fluctuations were 0.01 nm, which were less than the OSA resolution of 0.05 nm but within the data sampling interval of 0.01nm. These measurement results indicated that the TDFL can operate stably at a single wavelength over a 60-min measurement time.

Meanwhile, to demonstrate SLM operation of the proposed TDFL, self-homodyne measurement was carried out. The measurement setup included a 1 GHz photodetector (CONQUER KG-PR-1G-20) with a strong response in the 2 μm band and an 8 GHz radio-frequency (RF) electrical spectrum analyzer (ESA, R&SFSH8 handheld spectrum analyzer). The measured RF spectra of every lasing wavelength reflected by SFBG1 and SFBR2 are shown in Fig. 6(a) and (b), where the scanning ranges were set to 0–500 MHz and 0–1 GHz. No beating signal was captured for every lasing wavelength, and the laser operated in a stable SLM state. Still, repeated scans of the ESA during a 30-min period were taken to measure the stability for each lasing wavelength. No beat frequency signal was observed, which confirms that the laser was working at a stable SLM operation. To verify the capability of the DRCC, the RF beating spectra of the laser without the DRCC filter spliced inside the cavity were measured for one of the lasing outputs reflected by SFBG1 and are shown in Fig. 6(c). The numerous spikes in the spectra indicate lasing in the multi-longitudinal modes.

To further investigate the linewidth characteristics of the proposed TDFL, an imbalanced Michelson interferometer (MI) composed of a 3 $\times$ 3 coupler and two Faraday rotation mirrors (FRMs) was set for laser phase noise demodulation [16], [17]. A 50-m length standard single-mode fiber (SMF) was incorporated in an interferometer instead of the overlong delay line that has to be used in the traditional delayed self-heterodyne linewidth measurement method, as the transmission loss of 2 μm light is high. The received interference fringes, containing information about differential phase fluctuation accumulated in the delay time τ of the MI, were uploaded to a computer using an oscilloscope to calculate the power spectral density (PSD) of the instantaneous phase fluctuation and frequency fluctuation of the laser. Then the FWHM laser linewidth at different integration bandwidths was calculated based on the β-separation line method ($\beta = S_v(f) = (8 \ln 2/\pi^2) \cdot f$) [33]. Since the data acquisition system we used had a dynamic range limitation, the experimentally measured total frequency noise PSD was sliced by four segments of the frequency noise PSD measured at different time scales (1 s, 0.1 s, 0.01 s, and 0.001 s). In addition, since the data acquisition card we used was an 8-bit digital oscilloscope, the quantization noise is relatively large, which introduced a horizontal noise base on the right side of each frequency noise PSD spectrum after phase demodulation. To avoid ambiguities induced by this system

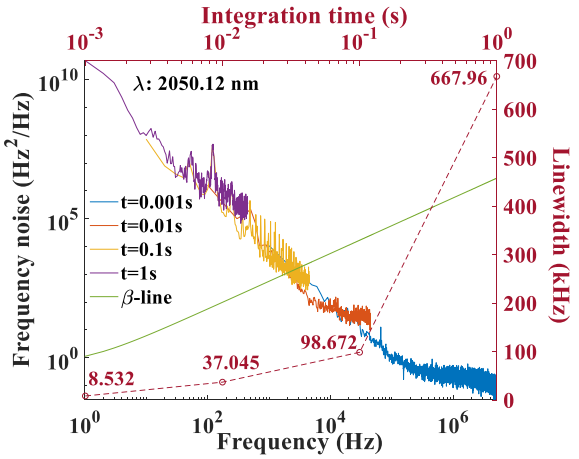

Fig. 7. Frequency noise PSD and FWHM linewidths at integration times ranging from 0.001 s to 1 s for 2050.12 nm wavelength.

TABLE II
FWHM LINEWIDTH FOR EACH WAVELENGTH AT DIFFERENT MEASUREMENT TIMES

t (s)	0.001	0.01	0.1	1
$\Delta\nu_{\lambda 11}$ (kHz)	9.204	59.347	82.811	705.64
$\Delta\nu_{\lambda 12}$ (kHz)	7.527	24.504	89.857	486.34
$\Delta\nu_{\lambda 13}$ (kHz)	8.532	37.045	98.672	667.96

noise, the noise base tails of the frequency noise PSD spectra measured at $t = 0.01$ s, 0.1 s, and 1 s were removed but the noise base at $t = 0.001$ s was kept. The measured frequency noise PSD and the calculated FWHM laser linewidth for the lasing output at 2050.12 nm are shown in Fig. 7. It can be seen from the spectrum that the overlap between the four frequency noise PSD segments was consistent. The FWHM linewidth increased upon increasing the measurement time (decreased integration bandwidth) since the divergence of $1/f$ noise led to a divergence of the integral area. Table II lists the linewidths of the measured lasing wavelengths at different measurement times. At the minimum measurement time (0.001 s), the maximum laser linewidth was about 9.2 kHz, and the maximum laser linewidth at the longest measurement time (1 s) was about 705 kHz. As we did not employ any vibration isolation, the technical noise generated from environmental vibrations and disturbances in the low-frequency range led to abnormally large linewidths at the maximum measurement time (corresponding to the sharp increase after $t = 0.1$ s). Moreover, the ~9 kHz linewidths at the minimum measurement time were mainly due to thermal noise from the thermal effect induced by cladding pumping and the noise from detectors. Nevertheless, the linewidths of the measured wavelengths were comparable with and even narrower than those from other works

A technical indicator comparison of our work to other proposed SLM TDFLs is shown in Table III. Since there are not many reports for the SLM TDFL at ~2050 nm, we mainly made the comparison for the laser at ~1.9 μm. Comparable and even better results observed for our laser showed the good performance of our proposed TDFL.

TABLE III
TECHNICAL INDICATOR COMPARISON OF OUR WORK TO OTHER PROPOSED SLM TDFLS

technique	Switch-ability	wavelength (nm)	Maximal power fluctuation	Maximal OSNR (dB)	linewidth
[34]	N	1950	1%	72	5.47 kHz
[23]	N	1957.24	NA	60	20 kHz
[35]	N	1978.6	NA	55	15.1 kHz
[36]	N	1950.06	NA	68	6.76 kHz
[37]	Y	1897	0.66 dB	25	9.1 MHz
this work	**Y**	**~2050**	**0.56 dB**	**72.11**	**9 kHz**

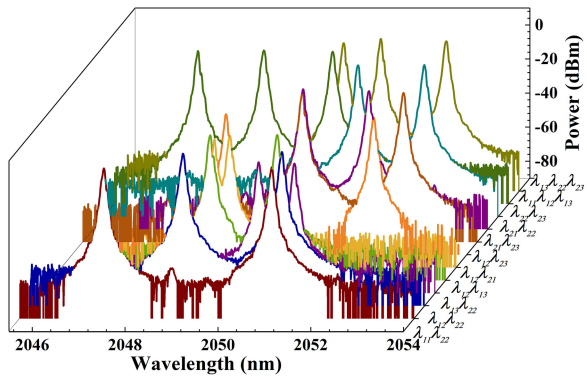

Fig. 8. Spectra of nine dual-wavelength ($\lambda_{11}\lambda_{22}$, $\lambda_{12}\lambda_{22}$, $\lambda_{13}\lambda_{22}$, $\lambda_{12}\lambda_{13}$, $\lambda_{12}\lambda_{21}$, $\lambda_{12}\lambda_{23}$, $\lambda_{21}\lambda_{23}$, $\lambda_{21}\lambda_{22}$, and $\lambda_{22}\lambda_{23}$), and two triple-wavelength ($\lambda_{11}\lambda_{12}\lambda_{13}$, $\lambda_{13}\lambda_{22}\,\lambda_{23}$) lasing operations.

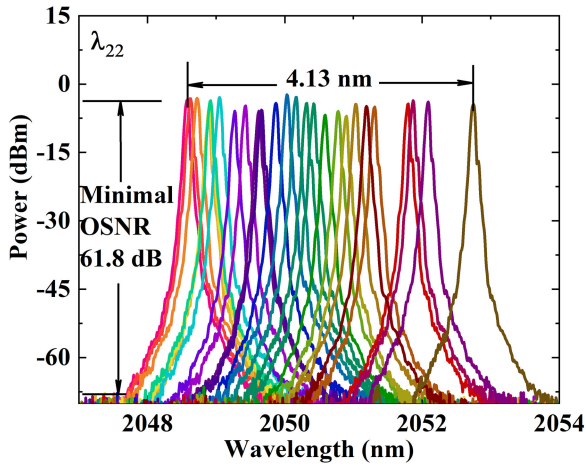

Fig. 9. Spectrum of the laser output reflected from the center reflection channel of SFBG2, with a wavelength-tunable range of ~4.13 nm.

B. Multi-Wavelength Operation

Apart from single-wavelength lasing, by carefully adjusting DI-PC1 and DI-PC2 in order, dual- and triple-wavelength lasing operation with the wavelength switched between six reflection channels was realized. The spectra of the obtained nine dual-wavelength and two triple-wavelength lasing operations are shown in Fig. 8. The OSNR of each was above 50 dB. As

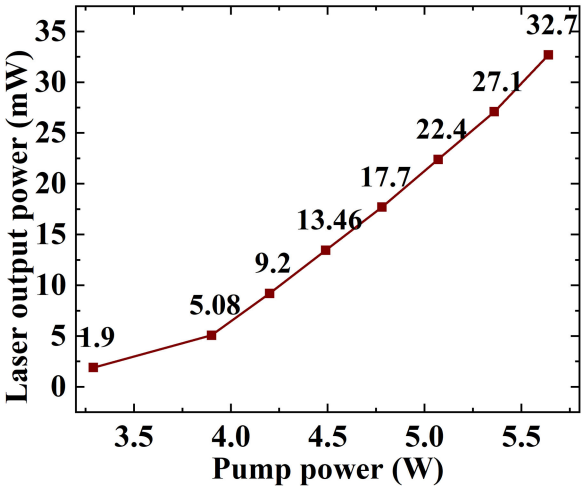

Fig. 10. Output power variation of the laser with different pump powers.

there was no extra mechanism for gain competition suppression in place of our laser system, the stability of dual-wavelength operation was worse than single-wavelength operation. Stable lasing was maintained for only over 20 min, and only several minutes for triple-wavelength lasing. However, by gently tuning the DI-PC, which controlled the SOP of the corresponding SFBG, stable dual- and triple-wavelength lasing could be recovered again.

The tunability of SFBG2 was investigated by tuning the right knob of the micro-displacement platform to impose the stain on SFBG2 in the horizontal direction. The operating wavelength at the center wavelength of SFBG2 of the fiber laser can be tuned from 2048.61 to 2052.74 nm continuously, as shown in Fig. 9, with a tunable range was as wide as ∼4.13 nm. The OSNR of the laser output within the wavelength-tunable range was no less than 61.8 dB. However, due to the overtightened fiber clamp and the fragility of the bare SFBG, the SBFG2 broke when the tuned wavelength was above 2052.7 nm. The wavelength-tunable range could be enlarged by recoating the fiber, and the longest operating wavelength at the longest wavelength channel of SFBG2 could be obtained by adjusting DI-PC2 and increasing the pump power.

Finally, the average power of the proposed TDFL was measured by the optical power meter (Ophir StarLite); the SOP in the cavity was not adjusted during measurement. Fig. 10 gave the average output power in variation with the pump power. The TDFL started to lase under single-wavelength operation with an output power of 1.9 mW when the pump power was 3.29 W, and the output power increased with the increasing pump power. When the pump power increased to 5.64 W, the output power was 32.7 mW. The slope efficiency of the laser was about 1.59%. The relatively low slope efficiency is mainly due to the low transmission of the subring cavity for SLM selection as well as the field mismatching loss caused by ion diffusion and size mismatch during fusion splicing between the hexagonal cross-section TDF and the pigtail of the FC and the circulator. It can be seen from the figure that the curve is not saturated. Considering the power-handling capability of the splicing point between the FC and the TDF, we did not further increase the pump power to test the limitations of output power.

IV. Conclusion

In summary, multi-wavelength switchable SLM TDFL lasing at ∼2050 nm was experimentally proposed. In the laser, two cascaded SFBGs were incorporated in the cavity to act as the six-wavelength channel reflector. Wavelength-switching was realized by adjusting the DI-PCs in front of the SFBGs to induce the different PDL of every reflection. A novel passive DRCC made with two symmetric 3 × 3 OCs was used for SLM selection, and the SLM selection ability of DRCC was theoretically analyzed and experimentally verified. The good laser output performances were also presented in detail. For the obtained six single-wavelength operations, the maximum OSNR was 72.11 dB, the maximum wavelength fluctuation was 0.01 nm, and the maximum power fluctuation was 0.56 dB. Every lasing output operated in a stable SLM state, and the measured laser linewidths were less than 9 kHz, which are comparable to the reported SLM lasers in this wavelength range. Nine dual-wavelength and two triple-wavelength operations were also realized. In addition, the tuning of SFBG2 made the TDFL be with a wavelength-tunable range of ∼4.13 nm. We believe that our proposed laser has great potential for application in free-space optical communication and next-generation lidar systems.

References

[1] S. W. Henderson and S. M. Hannon, "Advanced coherent lidar system for wind measurements," *Proc. SPIE 5887, Lidar Remote Sens. Environ. Monitor. VI*, Sep. 2005, vol. 5887.

[2] S. W. Henderson *et al.*, "Coherent laser radar at 2 mu m using solid-state lasers," *IEEE Trans. Geosci. Remote Sens.,* vol. 31, pp. 4–15, Jan. 1993.

[3] P. Kronenberg and O. Traxer, "The laser of the future: Reality and expectations about the new thulium fiber laser—A systematic review," *Transl. Androl Urol.,* vol. 8, pp. S398–S417, Sep. 2019.

[4] T. S. McComb *et al.*, "High-power widely tunable thulium fiber lasers," *Appl. Opt.,* vol. 49, pp. 6236–6242, Nov. 2010.

[5] X. Guan *et al.*, "55 W kilohertz-linewidth core- and in-band-pumped linearly polarized single-frequency fiber laser at 1950 nm," *Opt. Lett.,* vol. 45, pp. 2343–2346, Apr. 2020.

[6] S. Fu *et al.*, "Review of recent progress on single-frequency fiber lasers," *J. Opt. Soc. Amer. B,* vol. 34, pp. A49–A62, Mar. 2017.

[7] S. Fu *et al.*, "Linewidth-narrowed, linear-polarized single-frequency thulium-doped fiber laser based on stimulated Brillouin scattering effect," *IEEE Photon. J.,* vol. 9, May 2017, Art. no. 1504207.

[8] J. Geng, Q. Wang, J. Wang, S. Jiang, and K. Hsu, "All-fiber wavelength-swept laser near 2 μm," *Opt. Lett.*, vol. 36, pp. 3771–3773, Oct. 2011.

[9] J. Wu, Z. Yao, J. Zong, A. Chavez-Pirson, N. Peyghambarian, and J. Yu, "Single-frequency fiber laser at 2.05 um based on ho-doped germanate glass fiber," in *Proc. Fiber Lasers VI: Technol., Syst., Appl.*, 2009, vol. 7195, pp. 358–364.

[10] J. Geng *et al.*, "Single-frequency gain-switched Ho-doped fiber laser," *Opt. Lett.,* vol. 37, pp. 3795–3797, Sep. 2012.

[11] M. R. K. Soltanian, H. Ahmad, A. Khodaie, I. S. Amiri, M. F. Ismail, and S. W. Harun, "A stable dual-wavelength thulium-doped fiber laser at 1.9 μm using photonic crystal fiber," *Sci. Rep.,* vol. 5, Oct. 2015, Art. no. 14537.

[12] T. Feng *et al.*, "Four-wavelength-switchable SLM fiber laser with sub-kHz linewidth using superimposed high-birefringence FBG and dual-coupler ring based compound-cavity filter," *Opt. Exp.,* vol. 27, pp. 36662–36679, Dec. 2019.

[13] T. Feng, D. Ding, Z. Zhao, H. Su, F. Yan, and X. S. Yao, "Switchable 10 nm-spaced dual-wavelength SLM fiber laser with sub-kHz linewidth and high OSNR using a novel multiple-ring configuration," *Laser Phys. Lett.,* vol. 13, Aug. 2016, Art. no. 105104.

[14] S. Feng, S. Lu, W. Peng, Q. Li, T. Feng, and S. Jian, "Tunable single-polarization single-longitudinal-mode erbium-doped fiber ring laser employing a CMFBG filter and saturable absorber," *Opt. Laser Technol.,* vol. 47, pp. 102–106, Apr. 2013.

[15] B. Yin, S. Feng, Z. Liu, Y. Bai, and S. Jian, "Tunable and switchable dual-wavelength single polarization narrow linewidth SLM erbium-doped fiber laser based on a PM-CMFBG filter," *Opt. Exp.,* vol. 22, pp. 22528–22533, Sep. 2014.

[16] W. Han *et al.*, "Wavelength-switchable single-longitudinal- mode thulium-doped fiber laser with sampled fiber Bragg grating," *IEEE Access,* vol. 9, pp. 62212–62218, Apr. 2021.

[17] L. Zhang *et al.*, "Six-wavelength-switchable narrow-linewidth thulium-doped fiber laser with polarization-maintaining sampled fiber Bragg grating," *Opt. Laser Technol.,* vol. 136, 2021, Art. no. 106788.

[18] A. A. Jasim, M. Dernaika, S. W. Harun, and H. Ahmad, "A switchable figure eight erbium-doped fiber laser based on inter-modal beating by means of non-adiabatic microfiber," *J. Lightw. Technol.,* vol. 33, pp. 528–534, 2015.

[19] Y. Qi *et al.*, "Wavelength-switchable fiber laser based on few-mode fiber filter with core-offset structure," *Opt. Laser Technol.,* vol. 81, pp. 26–32, Jul. 2016.

[20] T. Feng *et al.*, "C-band 41-wavelength-switchable single-longitudinal-mode fiber laser with sub-kHz linewidth and high stability using a wide-band chirped moiré fiber Bragg grating," *Laser Phys. Lett.,* vol. 16, Jan. 2019, Art. no. 025106.

[21] Y. Li, Y. Shen, J. Tian, Q. Fu, and Y. Yao, "Wavelength switchable multi-wavelength erbium-doped fiber laser based on polarization-dependent loss modulation," *J. Lightw. Technol.,* vol. 39, pp. 243–250, 2021.

[22] W. Zheng, S. Ruan, M. Zhang, W. Liu, Y. Zhang, and X. Yang, "Switchable multi-wavelength erbium-doped photonic crystal fiber laser based on nonlinear polarization rotation," *Opt. Laser Technol.,* vol. 50, pp. 145–149, Sep. 2013.

[23] T. Yin, Y. Song, X. Jiang, F. Chen, and S. He, "400 mW narrow linewidth single-frequency fiber ring cavity laser in 2 um waveband," *Opt. Exp.,* vol. 27, pp. 15794–15799, May 2019.

[24] T. Yin, Y. Wei, and W. Mei, "Widely wavelength-tunable single-longitudinal-mode thulium-doped fiber laser incorporating a saturable absorber," in *Proc. 2017 Asia Commun. Photon. Conf.*, 2017, pp. 1–3.

[25] S. Feng, Q. Mao, Y. Tian, Y. Ma, W. Li, and L. Wei, "Widely tunable single longitudinal mode fiber laser with cascaded fiber-ring secondary cavity," *IEEE Photon. Technol. Lett.,* vol. 25, pp. 323–326, Jan. 2013.

[26] T. Feng, D. Ding, F. Yan, Z. Zhao, H. Su, and X. S. Yao, "Widely tunable single-/dual-wavelength fiber lasers with ultra-narrow linewidth and high OSNR using high quality passive subring cavity and novel tuning method," *Opt. Exp.,* vol. 24, pp. 19760–19768, Aug. 2016.

[27] T. Feng, M. Wang, X. Wang, F. Yan, Y. Suo, and X. S. Yao, "Switchable 0.612-nm-spaced dual-wavelength fiber laser with sub-KHz linewidth, ultra-high OSNR, ultra-low RIN, and orthogonal polarization outputs," *J. Lightw. Technol.,* vol. 37, pp. 3173–3182, Jul. 2019.

[28] T. Feng *et al.*, "Four-wavelength ultra-narrow linewidth fiber laser enabled by a figure-8 compound-ring-cavity filter and a polarization-managed four-channel filter," *Opt. Express*, vol. 29, pp. 31179–31200, 2021.

[29] J. Tian, Y. Yao, J. J. Xiao, X. Xu, and D. Chen, "A pump power controlled multiwavelength fiber laser with adjustable output channels at fixed wavelength," *Appl. Phys. B,* vol. 102, pp. 545–549, Mar. 2011.

[30] C.-C. Lee, Y.-K. Chen, and S.-K. Liaw, "Single-longitudinal-mode fiber laser with a passive multiple-ring cavity and its application for video transmission," *Opt. Lett.,* vol. 23, pp. 358–360, Mar. 1998.

[31] Z. Jianluo, Y. Chao-Yu, G. W. Schinn, W. R. L. Clements, and J. W. Y. Lit, "Stable single-mode compound-ring erbium-doped fiber laser," *J. Lightw. Technol.,* vol. 14, pp. 104–109, 1996.

[32] Z. Jianluo and J. W. Y. Lit, "All-fiber compound ring resonator with a ring filter," *J. Lightw. Technol.,* vol. 12, pp. 1256–1262, 1994.

[33] G. Di Domenico, S. Schilt, and P. Thomann, "Simple approach to the relation between laser frequency noise and laser line shape," *Appl. Opt.,* vol. 49, pp. 4801–4807, Sep. 2010.

[34] Q. Yang *et al.*, "A single-frequency linearly polarized fiber laser using a newly developed heavily tm3+-doped germanate glass fiber at 1.95 μm," *Chin. Phys. Lett.,* vol. 32, Sep. 2015, Art. no. 094206.

[35] J. N. Zhang, W. C. Yao, H. T. Wang, W. Zhou, X. Wu, and D. Y. Shen, "A watt-level single-frequency fiber laser at 2 μm using a silica prolate microresonator," *IEEE Photon. Technol. Lett.,* vol. 31, pp. 1241–1244, Jun. 2019.

[36] X. He *et al.*, "1.95 μm kHz-linewidth single-frequency fiber laser using self-developed heavily tm3+-doped germanate glass fiber," *Opt. Exp.,* vol. 21, pp. 20800–20805, Sep. 2013.

[37] W. Yang *et al.*, "A novel switchable and tunable dual-wavelength single-longitudinal-mode fiber laser at 2 μm," *IEEE Photon. Technol. Lett.*, vol. 28, pp. 1161–1164, Feb. 2016.